Heliyon 10 (2024) e34684

Contents lists available at ScienceDirect

Heliyon

journal homepage: www.cell.com/heliyon

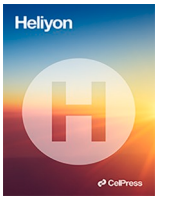

Research article

A broadband modulator based on graphene/black phosphorus heterostructure with enhanced modulation depth

Feng Zhou

College of Media Engineering, Communication University of Zhejiang, Hangzhou, 310018, China

ARTICLE INFO

Keywords:
Graphene/black phosphorus heterostructure
Surface plasmon polaritons
Large waveband
Few-layer graphene
Enhanced modulation depth
Angle dependence

ABSTRACT

We theoretically present a broadband modulator based on graphene/black phosphorus heterostructure which can work over a large waveband from visible (VIS) to mid-infrared (MIR) regions. By utilizing the angle dependence of black phosphorus, surface plasmon polaritons (SPP) modulation can be achieved in VIS regime, while the wavelength is tuned within the near-infrared (NIR) or MIR regions, the enhanced modulation depth can be achieved by few-layer graphene films. Results show that the proposed plasmonic modulator exhibits a broad waveband from 400 nm to 3 μm. In addition, this proposed modulator features high modulation depth (MD), low insertion loss (IL), large 3-dB modulation bandwidth and small power consumption from VIS to MIR regions. Our work may extend the operation waveband of opto-electro devices based on the hybridized 2D materials and would promote their potential future applications.

1. Introduction

In recent years, graphene-based optical waveguide modulators have been intensively researched and demonstrated due to the extraordinary properties of graphene, including the ultrafast carrier mobility, tunable tunability and sound compatibility with Complementary Metal Oxide Semiconductor (CMOS) [1–4]. To further address the issue of weak light-matter interaction in this modulator, surface plasmon polariton (SPP) has been proposed as a solution to enhance the light-matter interaction, and massive research of modulators based on graphene surface plasmons (GSP) have been studied, including the all-optical plasmonic modulators [5–11]. Apart from SPP, few layers graphene has also been exploited to optimize light-matter interaction in graphene-based modulators [12,13]. Although GSP has been widely used in the modulation application and exhibits excellent performances, modulators working in the visible (VIS) regime are rarely investigated and due to the relatively small modulation depth (MD) in mid-infrared (MIR) regions, there is still no report of graphene-based modulator that can work through a large waveband from VIS to MIR regime.

In fact, black phosphorus has a tunable direct bandgap (0.3 eV–2 eV) which can compensate graphene, indicating that black phosphorus has the potential to work through a large waveband from VIS to MIR regions [14–16]. With the fast pace of van der Waals heterostructures' research, graphene/black phosphorus heterostructure has drawn a lot of interest and focus amongst the research field [17–21], and the combination of them into the graphene/black phosphorus heterostructure may usher into some interesting phenomena and functions. Various devices have been designed and investigated based on graphene/black phosphorus heterostructure, including photodetectors [22,23], field effect transistors (FET) [24], and absorbers [25,26]. Recently, SPP characteristics of graphene/black phosphorus heterostructure have also been investigated and utilized to achieve certain devices [27,28], which would contribute to manipulating light at nanoscale by further enhancing the light-matter interaction via SPP. Besides, black phosphorus

E-mail address: 20150029@cuz.edu.cn.

https://doi.org/10.1016/j.heliyon.2024.e34684
Received 5 May 2023; Received in revised form 10 July 2024; Accepted 15 July 2024
Available online 15 July 2024

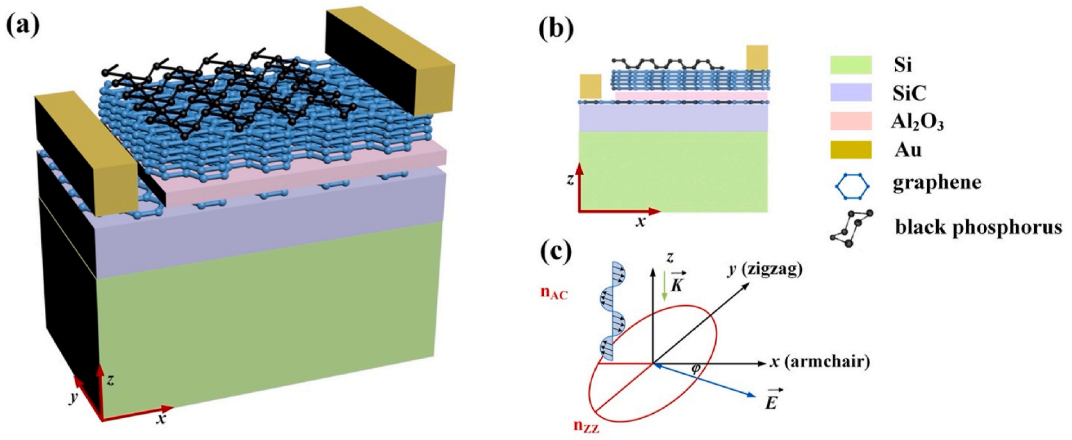

Fig. 1. Diagram of the proposed graphene/black phosphorus modulator. (a) 3D schematic view of the modulator; (b) cross sectional view of the modulator; (c) the in-plane anisotropy of black phosphorus.

owns strong in-plane anisotropy and exhibits the angle dependence in the SPP characteristics [29,30]. Therefore, through tuning SPP characteristics of graphene/black phosphorus heterostructure, the advantages of both materials would be creatively combined while the bottlenecks of both materials would be compensated. Lately, we have presented an all-optical plasmonic modulator based on graphene/black phosphorus heterostructure which could work within the VIS regime [31]. However, how to extend the modulator waveband from VIS to MIR regime is still a challenge.

In this paper, we proposed a broadband modulator based on graphene/black phosphorus heterostructure with enhanced MD. By actively tuning the incident light angle of black phosphorus, this plasmonic modulator was configured in an all-optical way within the VIS regime. On the other hand, in near-infrared (NIR) and MIR regions, five-layer graphene has been utilized to further enhance the MD, this plasmonic modulator was functioning in an electro-optic modulation way. Comparing to the recently reported all-optical plasmonic modulator [31], the proposed modulator could operate form 400 nm to 3 μm, spanning from VIS to MIR regimes. Besides, it also addressed the issue of weak MD in MIR regime. As a result, this proposed plasmonic modulator featured large ER, MD, and 3-dB modulation bandwidth as well as small insertion loss (IL) and power consumption, which would provide potential methods in building and optimizing angle-dependent plasmonic devices in future nanophotonics.

2. Principle and device structure

Fig. 1(a) shows the proposed broadband graphene/black phosphorus modulator featuring few-layer graphene films. The whole modulator is constructed onto the Si/SiC substrate whose length l and height h are 800 nm and 400 nm, respectively, among which the height of Si and SiC is 350 nm and 50 nm, respectively. The refractive indices of Si and SiC are 3.46 and 2.57, respectively. The heterostructure consists of the mono-layer graphene, Al_2O_3, five-layer graphene and black phosphorus from bottom to top view, and the cross-sectional view of the proposed modulator is depicted in Fig. 1(b). The refractive index and thickness of Al_2O_3 film are set as 1.746 and 10 nm, respectively. The thickness of mono-layer graphene and black phosphorus are both specified as 0.34 nm. Two Au electrodes are each 100 nm in height and connected to the top and bottom graphene sheets, respectively.

In practical manufacturing, graphene sheets can be prepared by chemical vapor deposition (CVD) method and formed by the standard UV lithography. The mono-layer graphene sheet is first transferred on the SiC as the bottom graphene layer, Al_2O_3 film of 10 nm thickness is then uniformly deposited on the bottom mono-layer graphene sheet, since its adhesion and conductivity are in sound accordance with the graphene layer, the five-layer graphene films are then transferred onto the Al_2O_3 film, serving as the top graphene sheets. Black phosphorus can be mechanically exfoliated onto Polydimethylsiloxane (PDMS), and attached to the three-axis micrometer stage. Then immediately, black phosphorus on PDMS is positioned upside down and transferred on top graphene sheets using three-axis micrometer stage and optical microscope, removing the PDMS film. Standard UV lithography and oxygen plasma etching techniques are used to define the area of the graphene/black phosphorus heterostructure. In addition, by metal deposition and liftoff process, two Au electrodes can be deposited and connected to the top and bottom graphene sheets, respectively. Thus, by exerting applied voltage on the top and bottom graphene sheets, optical properties of the whole heterostructure would be accordingly tuned.

Based on the proposed graphene/black phosphorus heterostructure, we first studied the SPP modulation capability in VIS regime. According to the SPP theory and Kubo formula [32], the minimum chemical potential of graphene μ_c to stimulate SPP waves through the VIS regime was calculated to be from 1.06 eV ($\lambda = 780$ nm) to 2.32 eV ($\lambda = 400$ nm), here we set μ_c as 2.5 eV. The dispersion of proposed graphene/black phosphorus heterostructure was investigated and derived as [32,33]:

$$k_{SPP} = \frac{\pi\hbar^2}{e^2\mu_c}\varepsilon_0(\varepsilon_r + \varepsilon_{BP})\omega\left(\omega + \frac{i}{\tau}\right) \tag{1}$$

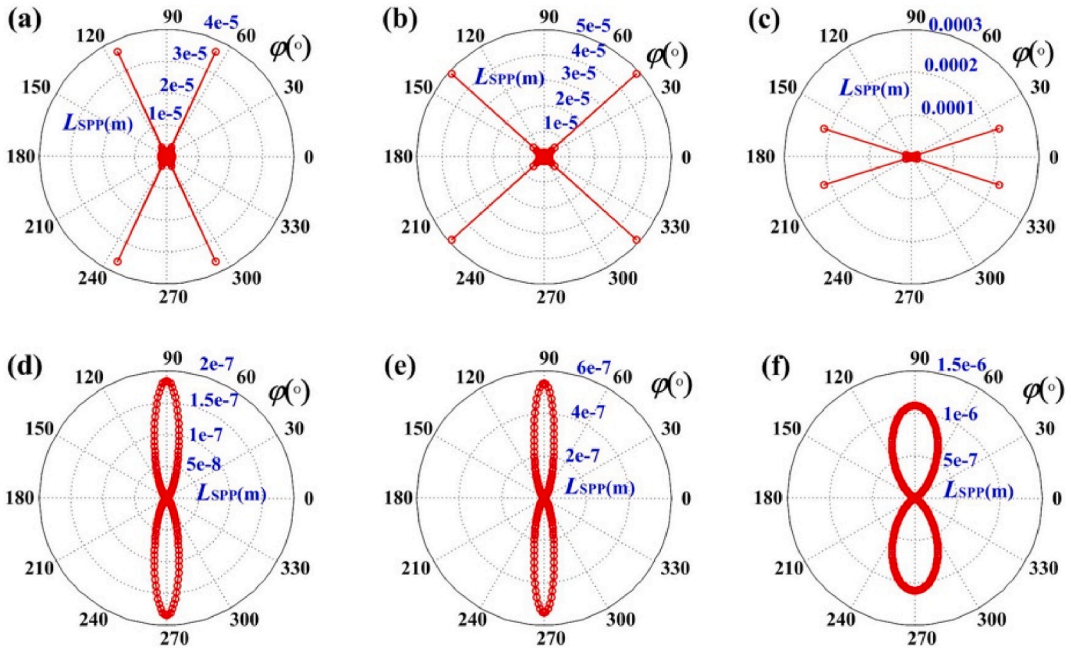

Fig. 2. (a) The relationship between L_{SPP} and ϕ in VIS regime for (a) 400 nm, (b) 450 nm, (c) 487 nm, (d) 600 nm, (e) 700 nm, and (f) 780 nm.

Where ε_{BP} and ε_r indicate the dielectric constant of black phosphorus and SiC, respectively, and ω is the optical frequency. It should be noted that ε_{BP} is composed of real (ε'_{BP}) and imaginary part (ε''_{BP}), which vary with the wavelength. ε_{BP} is composed of three components in x (armchair), y (zigzag) and z axes. By presuming ϕ to be the angle between the incident light and the armchair direction, it can be derived that ε_{BP} is angle-dependent, and according to Eq (1), dispersion of the proposed modulator is also dependent on ϕ. Thus, by rotating ϕ, the stimulated SPP wave is dependently dispersive, which reveals the mechanism of SPP modulation by simply optically tuning ϕ, and gives the possibility of realizing SPP modulator in VIS regime based on the graphene/black phosphorus heterostructure. As for SPP modulation, one of the uttermost important characterized parameters is the SPP propagation length L_{SPP}, which is decided by the imaginary part of SPP wave vector [33], shown as:

$$L_{SPP} = \frac{1}{2k''_{SPP}} = \frac{e^2\mu_c}{2\pi\hbar^2\varepsilon_0\omega}\left[\left(\frac{\varepsilon_r + \varepsilon'_{BP}}{\tau}\right) + \varepsilon''_{BP}\omega\right]^{-1} \tag{2}$$

From Eq (2), it can be seen that L_{SPP} is dependent with ε_{BP} which varies with the wavelength and ϕ. Thus, it would be interesting to study the angle dependence of the SPP properties for the proposed modulator. In addition, since black phosphorus is a biaxial crystal featuring the evident in-plane anisotropy, as shown in Fig. 1(c), the effective refractive index of black phosphorus is decided by both values from armchair ($\boldsymbol{n}_{AC}$) and zigzag ($\boldsymbol{n}_{ZZ}$) directions, which form an elliptical shape [34]. Based on this, the relationship between ε_{BP} and ϕ can be expressed by Eq (3):

$$\boldsymbol{\varepsilon}_{BP}(\phi) = \frac{\boldsymbol{\varepsilon}_{AC}\boldsymbol{\varepsilon}_{ZZ}}{\boldsymbol{\varepsilon}_{AC}\,sin^2(\phi) + \boldsymbol{\varepsilon}_{ZZ}\,cos^2(\phi)} \tag{3}$$

3. Simulation results and discussions

By using the finite element analysis (FEA) method via COMSOL Multiphysics, we numerically investigated the proposed modulator. When the proposed all-optical modulator is working in the visible regime, as shown in Fig. 1(c), the periodic boundary conditions are applied along the x (armchair) and y (zigzag) directions, and the perfectly matched layer boundary conditions are employed in the z direction. A polarized light with input power of 1W in a period and electric field perpendicular to the black phosphorus layer vertically irradiates upon the heterostructure. Similarly, when the modulator is working in the NIR and MIR regimes, mode analysis with scattering boundary is employed to calculate the effective modal index of the heterostructure, and the 2D frequency-domain field and power monitors are used to obtain the electric field distributions. For both situations, the non-uniform mesh is adopted in the simulation regions to save storage space and computing time [35]. The maximum element mesh size is set as 0.1 nm inside the graphene and black phosphorus layers. The mesh size gradually increases outside the graphene and black phosphorus layers.

Here we first studied the all-optical plasmonic modulator working within the VIS regime. The normal incident light with linear polarization ϕ perpendicularly irradiated onto the black phosphorus layer, with the dynamic tuning of ϕ, L_{SPP} could be tuned to realize either ON or OFF state of the modulation. The relationships between L_{SPP} and ϕ within the VIS regime from 400 nm to 780 nm are

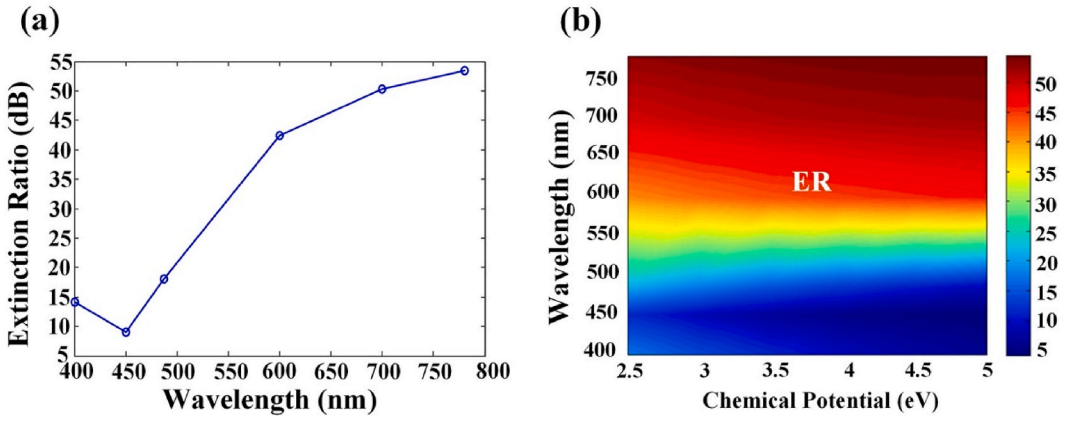

Fig. 3. (a) The largest ER for our proposed modulator by just tuning ϕ in VIS regime; (b) The relationship between ER and μ_c in the whole VIS regime.

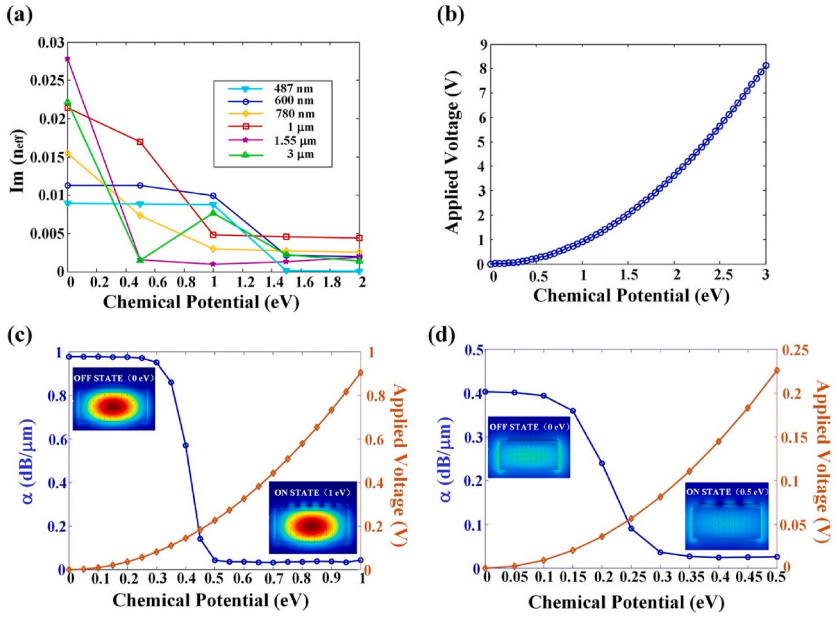

Fig. 4. (a) Im(n_{eff}) of the proposed modulator varying with from VIS to MIR regime; (b) The relationship between the applied voltage and chemical potential μ_c; Dependence of attenuation a on chemical potential μ_c and applied voltage on chemical potential μ_c at the wavelength of (c) 1.55 μm and (d) 3 μm, respectively. The inset figures show the electric field profiles for TM mode at ON and OFF states, respectively.

shown in Fig. 2(a)-(f).

From Fig. 2, it can be observed that throughout the VIS regime, L_{SPP} exhibits the π symmetry, and holds the potential of obtaining large discrepancy within small rotation of ϕ. To be more specific, when the wavelength is swept at 400 nm, as shown in Fig. 2(a), the largest L_{SPP} of 36.3 μm is obtained by rotating ϕ to 65 °. However, when ϕ is rotated to 66 °, the smallest L_{SPP} of 0.193 μm can be achieved, and a large discrepancy of 189 times is obtained with just rotation of 1 °. It is noteworthy that the largest and smallest value of L_{SPP} is not observed either in the armchair or zigzag direction. Interestingly, by sweeping the wavelength from 400 nm to 487 nm, the desired ϕ of obtaining the maximum or minimum value of L_{SPP} varies, as shown in Fig. 2(b) and (c). Nevertheless, at the wavelengths over 600 nm, displayed from Fig. 2(d)–(f), the maximum and minimum value of L_{SPP} occur at zigzag and armchair direction, respectively. This phenomenon can be explained by ε_{BP} within the VIS regime, from around 400 nm–487 nm, Im(ε_{BP}) in the armchair direction is negligent as 0, which would almost contribute zero absorption, in this case, the loss is mainly contributed by Im(ε_{BP}) in the zigzag direction. However, from 487 nm to 780 nm, Im(ε_{BP}) in armchair direction gradually rises to the sizable value, which in turn would contribute dominant loss of SPP wave propagation, and in this situation, when ϕ is tuned at 0 °, the stimulated SPP wave would be blocked in the propagation. A certain propagation length L is introduced to obtain the extinction ratio (ER) by calculating the transmission of ON and OFF states of the proposed modulator, displayed as $ER = 20\,lg\frac{T_{ON}}{T_{OFF}}$, and the transmission function can be

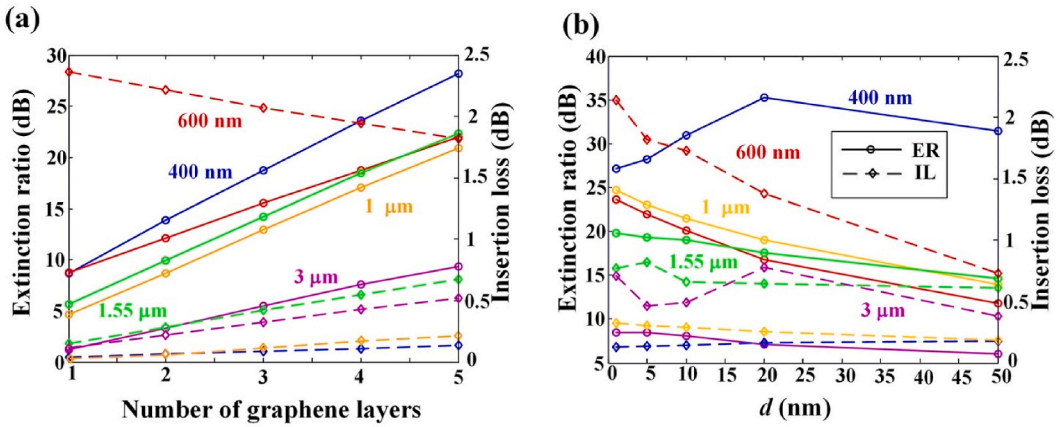

Fig. 5. ER (solid lines) and IL (dash lines) of the proposed modulator varying with (a) the layer number of graphene sheets; (b) the thickness of Al_2O_3 layer d from VIS to MIR regions.

obtained by $T = \int_0^L \exp(-L/L_{SPP})dL$. By positioning the maximum and minimum value of L_{SPP} via rotating ϕ, the largest ER can be obtained. We calculated and sketched the largest achievable ER within VIS regime, as shown in Fig. 3(a). It can be seen that from 400 nm to 780 nm, the largest ER mainly increases with the wavelength except at 450 nm, and especially when the wavelength is tuned at over 600 nm, the largest ER of over 40 dB can be obtained, which is of great importance to construct the modulator. Besides, since graphene provides the possibility to dynamically tune its Fermi energy, we also took into considerations of how graphene's Fermi energy made contributions to ER, and we studied the relationship between ER and μ_c in VIS regime. Results are illustrated in Fig. 3(b), with the increase of graphene's Fermi energy, ER is gradually improved in the whole VIS regime. Therefore, in VIS regime, by just tuning ϕ, modulation with large ER can be achieved in an all-optical way. However, when it comes to the NIR and MIR regions, by rotating ϕ, it is found that the largest and smallest L_{SPP} always appear at zigzag and armchair direction, respectively. And the discrepancy of the largest and smallest L_{SPP} is greatly shrinking, which means that ER of the proposed all-optical modulator is significantly decreasing and the mechanism of modulator based on angle-dependent tunability is not functioning in NIR and MIR regions.

To extend the wavelength to NIR and MIR regions, few-layer graphene sheets can be alternately employed to enhance MD of the proposed modulator, by actively tuning the applied voltages of top and bottom graphene sheets, electro-optic modulation can be also achieved with improved MD. Simulative computations were conducted by COMSOL Multiphysics, and the incident light was from the waveguide cross-section (in the $y-z$ plane of the proposed modulator as shown in Fig. 1). Here we used five-layer graphene as the top graphene sheets. By actively tuning μ_c, $\mathrm{Im}(n_{eff})$ of the proposed modulator from VIS to MIR regimes is accordingly changed, as shown in Fig. 4(a). According to the attenuation expression $\alpha = 20k_0 \times \lg(1/e) \times \mathrm{Im}(n_{eff})$, different attenuations of the proposed modulator can be achieved by varying μ_c. Since μ_c can be adjusted by varying the applied voltage, to evaluate the switching voltage, the relation between applied voltage and μ_c can be obtained as: $\mu_c = \hbar V_F \sqrt{\eta\pi|V_0 - V_D|}$, where $V_D = 0.8$ V [36], η is derived by $\eta = \frac{\varepsilon_0 \varepsilon_d}{ed}$. Fig. 4(b) shows the relationship between the applied voltage and μ_c of graphene for the proposed modulator. Based on these results, the dependence of attenuation α on μ_c and applied voltage on μ_c at wavelength of 1.55 μm (NIR regime) and 3 μm (MIR regime) is illustrated in Fig. 4(c) and (d), respectively. The inset figures show the electric field profiles for TM mode at ON and OFF states, respectively. When the wavelength is swept to 1.55 μm in NIR regime, by adjusting μ_c of graphene sheets as 0 eV, the maximum value of α is achieved with around 0.977 dB/μm, which can be regarded as the OFF state. However, when μ_c is switched to 1 eV, the minimum value of α is obtained with around 0.035 dB/μm, which can be regarded as the ON state. Consequently, MD of the proposed modulator is calculated to be about 0.942 dB/μm by actively tuning μ_c from 0 eV to 1 eV, indicating that only 0.9 V of the switching voltage is required, as shown in Fig. 4(c). With the same method, as for the wavelength of 3 μm in MIR regime, depicted in Fig. 4(d), by tuning μ_c as 0 eV, the maximum α of 0.403 dB/μm is obtained (OFF state), while μ_c is adjusted to 0.5 eV, the minimum α is 0.026 dB/μm (ON state), and MD of our proposed modulator is calculated to be about 0.377 dB/μm, which is equivalent of the tuning of applied voltage with only 0.23 V.

In addition, we also investigated how the number of graphene layers influenced ER and insertion loss (IL) of the proposed modulator. We calculated and obtained the corresponding ER and IL values for different numbers of graphene layers, ranging from the VIS to MIR regions, as shown in Fig. 5(a). It is found out that both ER and IL increase linearly with the number of graphene layers, except at the wavelength of 600 nm, when ER (red solid line) and IL (red dash line) exhibit the linear trade-off relationship. This is caused by the significant imaginary part of permittivity of black phosphorus in armchair direction at the wavelength of 600 nm, which plays the dominant role in deciding the total loss of the proposed modulator working at OFF state. Taking wavelength of 1.55 μm as an example, the calculated ER values (green solid line) are 5.69, 9.91, 14.21, 18.51 and 22.32 dB for mono-, bi-, tri-, quadri- and five-layer graphene, respectively; while IL values (green dash line) are calculated to be 0.151, 0.285, 0.419, 0.551 and 0.673 dB for mono-, bi-, tri-, quadri- and five-layer graphene, respectively. In this situation, choosing five-layer graphene sheets would significantly enhance the light-matter interaction and ER without causing too much damage of IL indicator.

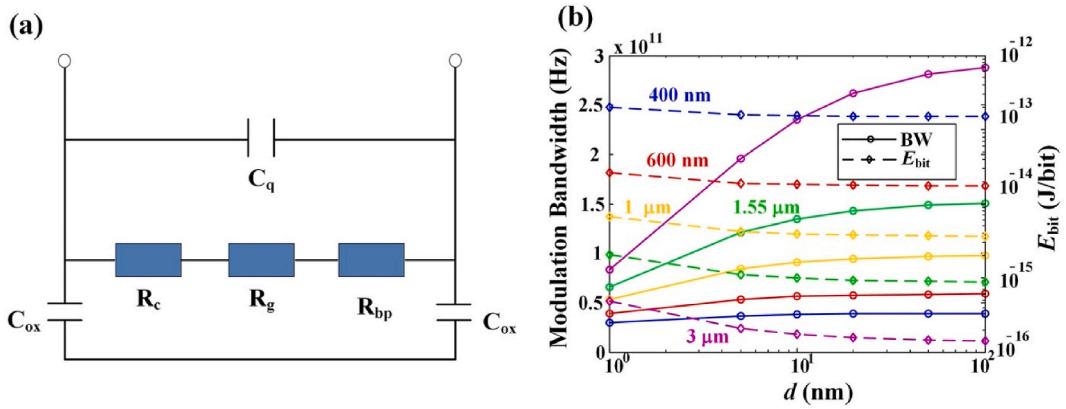

Fig. 6. (a) The equivalent electrical circuit of the proposed modulator; (b) modulation bandwidth (solid lines) and power energy (dash lines) of the proposed modulator varying with the thickness of Al_2O_3 layer d from VIS to MIR regions.

Apart from the number of graphene layers, we also studied how the thickness of Al_2O_3 layer d affected the ER and IL from VIS to MIR regions. Here we set d from 1 nm to 50 nm. Results are shown in Fig. 5(b), ER (solid lines) and IL (dash lines) exhibit different trends with d as the wavelength changes. As for ER, when the wavelength is tuned at 400 nm, ER (blue solid line) first experiences the uplifting trend with increase of d before reaching its peak at $d = 20$ nm, and then it decreases as d continues to increase. For other wavelengths, ER curves consistently display the decreasing trend as d increases. On the other hand, regarding IL, the IL curves exhibit different trends for various wavelengths as d increases, but with the largest value smaller than 2.5 dB.

Besides ER and IL, modulation bandwidth and power consumption are also two important parameters for the proposed modulator. The thickness of Al_2O_3 layer d of our proposed heterostructure would exert influences onto the 3-dB modulation bandwidth and power consumption. Thus, we also took these two parameters into considerations. As for our proposed modulator, when it worked on the VIS regime, we stimulated SPP and utilized the rotation of ϕ to achieve modulation with large ER in an all-optical way, going beyond the limitation of RC delay. However, when we adjusted μ_c of graphene to work in NIR and MIR regions, the RC constant became the dominant factor of modulation bandwidth. To calculate the cutoff 3-dB bandwidth, we used the expression $f = \frac{1}{2\pi R_t C_t}$, where R_t and C_t indicate the total resistance and capacitance, respectively. The equivalent electrical circuit is shown in Fig. 6(a), it can be found that R_t includes the contact resistance R_C, resistance of graphene R_g, and the resistance of black phosphorus R_{BP}, $\rho_C = R_C \bullet \frac{S}{h}$, where S and h represent the area and thickness of graphene sheet. Since extremely low graphene/metal contact resistances down to 20–150 Ω μm have been experimentally achieved [37], here R_C is chosen as 150 Ω μm. According to our proposed modulator, R_C is calculated relatively small that can be neglected. As for R_g, the regular value is regarded as 200 Ω/sq, and it can be calculated that for our proposed structure, R_g and R_{BP} are estimated to be about 50 Ω in total. Thus, R_t is estimated to be around 50 Ω C_t can be calculated by $C_t = (0.5C_{ox} + C_Q) \bullet A$ [38], where C_{ox} can be obtained by the parallel plate capacitor model, and C_Q can be derived by $C_Q = \frac{4\pi e^2 c}{hV_F^2 \lambda}$ [38], A is the overlapping area between the top and bottom graphene sheets, h and V_F represent the Planck constant and Fermi velocity, respectively. Therefore, C_t is dependent with the wavelength and the thickness of Al_2O_3 layer d. Taking wavelength of 1550 nm (green solid line) and d of 10 nm as an example, calculation results in our structure show that C_t is about 24 fF in the proposed modulator, resulting in a 3-dB modulation bandwidth of 135 GHz. By varying d, 3-dB modulation bandwidth would accordingly change. Here we set d from 1 nm to 100 nm, the relationship between the 3-dB modulation bandwidth and d starting from VIS to MIR regions is depicted in Fig. 6(b). To be more specifically, 3-dB modulation bandwidth (solid lines) increases with d for all the wavelengths and the largest 3-dB modulation bandwidth can be close to 300 GHz for the wavelength of 3 μm (purple solid line) when d is 100 nm. Meanwhile, the 3-dB modulation bandwidth also increases when the wavelength is swept from VIS to MIR regions. In real fabrication, by using the state-of-the-art process of the ultraviolet ozone optimization method, the modulation bandwidth would be further enlarged.

As for the power consumption, the power per bit (E_{bit}) was thereby taken into consideration. According to $E_{bit} = C(\Delta V)^2 / 4$, E_{bit} is related to C_t and the applied voltage, thus, for the proposed modulator, choosing wavelength of 1550 nm and d of 10 nm, E_{bit} can be estimated to 0.99 fJ/bit, which is much smaller than the conventional graphene-based modulators. With the same method, the relationships between E_{bit} and d starting from VIS to MIR regions are also depicted in Fig. 6(b). It can be found that the power consumption (dash lines) gradually decreases with d for all the wavelengths, meanwhile, the power consumption also decreases with the wavelength being swept from VIS to MIR regions.

Thus, it can be concluded that with the increase of d, 3-dB bandwidth of the proposed modulator increases while its power consumption decreases, considering the abovementioned ER and IL, it can be observed that ER, IL, 3-dB bandwidth and power consumption exhibit the trade-off relationship with d one another, to maintain the balance between ER, IL, 3-dB modulation bandwidth and power consumption, the value of 10 nm for d was chosen in our structure.

In addition, we categorized the performance of the recently-reported graphene-based plasmonic modulators (including the all-optical modulators based on nonlinear graphene plasmonics), as listed in Table 1 [5–11]. To measure the comprehensive performance of the modulators, several key parameters were considered for evaluation, including 3-dB modulation bandwidth (BW), ER, IL,

Table 1
The performance comparison of the graphene-based plasmonic modulators with our proposed modulator.

Reference	MD (dB/μm)	ER (dB)	IL (dB)	BW (GHz)	E_{bit} (fJ/bit)	Operation waveband
[5]	n/a	22	1.3	71	4.8	7 ~ 10 μm
[6]	0.5	n/a	n/a	127	72	1100–1900 nm
[7]	1.13	n/a	n/a	95	138.8	1200–1600 nm
[8]	3.12	n/a	0.66	380.23	29.39	1300–1800 nm
[9]	0.316	n/a	0.826	346	54.8	1200–1900 nm
[10]	0.28	3.5	6.2	>100	<600	1550 nm
[11]	0.875	3.5	19	n/a	35	1530–1560 nm
OURS	1.1	>15	<1	300	0.99	400 nm-3 μm

power consumption, and operation waveband.

It can be observed from Table 1, compared with the recent graphene-based plasmonic modulators, our proposed plasmonic modulator has advantages of relatively high ER, low insertion loss, large 3-dB modulation bandwidth, and small consumed power. Most notably, while all the proposed plasmonic modulators operate on the certain waveband, such as NIR or MIR regime, our proposed modulator can work over a large waveband from 400 nm to 3 μm, outperforming the other graphene-based plasmonic modulators. Specially, when it is working within the VIS regime via the all-optical configuration, the angle-dependent properties can be obtained and utilized to design the performance-tailored modulators. Overall, in the comprehensive evaluation of different parameters, our proposed modulator demonstrated relatively sound performance.

4. Conclusion

In summary, a broadband modulator based on graphene/black phosphorus heterostructure is proposed and demonstrated with a large waveband from VIS to MIR regions and enhanced modulator depth. By utilizing the angle-dependent SPP properties, the proposed modulator can be realized in an all-optical way in the VIS regime with large extinction ratio. Additionally, in the NIR and MIR regions, it exhibits the enhanced modulation depth with few-layer graphene films by actively tuning its chemical potential. Results show that the waveband of the proposed modulator can be extended from 400 nm to 3 μm with enhanced modulation depth, and it also enjoys the high extinction ratio, low insertion loss, large 3-dB modulation bandwidth and small power consumption. Our work may pave the way towards the future opto-electro devices with extended waveband and tunable angle-dependent characteristics realized by 2D van der Waals heterostructure.

Data availability statement

Data will be made available on request.

CRediT authorship contribution statement

Feng Zhou: Writing – review & editing, Writing – original draft, Methodology, Investigation, Funding acquisition.

Declaration of competing interest

The authors declare that they have no known competing financial interests or personal relationships that could have appeared to influence the work reported in this paper.

Acknowledgements

This work was supported by the Natural Science Foundation of Zhejiang Province under Grant No. LY23F050002 and the 5246 Talent Project of Zhejiang Province.

References

[1] E. Heidari, H. Dalir, F.M. Koushyar, B.M. Nouri, C. Patil, M. Miscuglio, D. Akinwander, V.J. Sorger, Integrated ultra-high-performance graphene optical modulator, Nanophotonics 11 (2022) 4011–4016, https://doi.org/10.1515/nanoph-2021-0797.
[2] Y. Ma, J. Li, Z. Han, H. Maeda, J. Pistora, All-dielectric graphene-induced T-slot waveguide electro-optic modulator with polarization-independent operation, IEEE J. Sel. Top. Quant. Electron. 27 (2021) 1–8, https://doi.org/10.1109/JSTQE.2021.3050569.
[3] M. Jin, Z. Wei, Y. Meng, H. Shu, Y. Tao, B. Bai, X. Wang, Silicon-based graphene electro-optical modulators[C], Photon 9 (2022) 82, https://doi.org/10.3390/photonics9020082.
[4] H. Dalir, Y. Xia, Y. Wang Y, X. Zhang, Athermal broadband graphene optical modulator with 35 GHz speed, ACS Photonics 3 (2016) 1564–1568, https://doi.org/10.1021/acsphotonics.6b00398.
[5] M.H. Rezaei, M. Shiri, High-performance tunable resonant electro-optical modulator based on suspended graphene waveguides, Opt Express 29 (2021) 16299–16311, https://doi.org/10.1364/OE.425599.
[6] S. Liu, M. Wang, T. Liu, Y. Xu, J. Yue, Y. Yi, X. Sun, D. Zhang, Polarization-insensitive graphene modulator based on hybrid plasmonic waveguide[C], Photon 9 (2022) 609, https://doi.org/10.3390/photonics9090609.

[7] M. Shirdel, M.A. Mansouri-Birjandi, Broadband graphene modulator based on a plus-shaped plasmonic slot waveguide, Appl. Opt. 58 (2019) 8174–8179, https://doi.org/10.1364/AO.58.008174.
[8] L. Ye, K. Sui, Y. Zhang, Q.H. Liu, Broadband optical waveguide modulators based on strongly coupled hybrid graphene and metal nanoribbons for near-infrared applications, Nanoscale 11 (2019) 3229–3239, https://doi.org/10.1039/C8NR09157A.
[9] Y. Zhu, C. Deng, L. Huang, G. Hu, B. Yun, R. Zhang, Y. Cui, Hybrid plasmonic graphene modulator with buried silicon waveguide, Opt Commun. 456 (2020) 124559, https://doi.org/10.1016/j.optcom.2019.124559.
[10] M. AlAloul, M. Rasras, Low insertion loss plasmon-enhanced graphene all-optical modulator, ACS Omega 6 (2021) 7576–7584, https://doi.org/10.1021/acsomega.0c06108.
[11] M. Ono, M. Hata, M. Tsunekawa, K. Nozaki, H. Sumikura, H. Chiba, M. Notomi, Ultrafast and energy-efficient all-optical switching with graphene-loaded deep-subwavelength plasmonic waveguides, Nat. Photonics 14 (2020) 37–43, https://doi.org/10.1038/s41566-019-0547-7.
[12] F. Zhou, C. Liang, The absorption ring modulator based on few-layer graphene, J. Opt. 21 (2019) 045801, https://doi.org/10.1088/2040-8986/ab0b35.
[13] A.A. Sayem, M.R.C. Mahdy, I. Jahangir, M.S. Rahman, Ultrathin ultra-broadband electro-absorption modulator based on few-layer graphene based anisotropic metamaterial, Opt Commun. 384 (2017) 50–58, https://doi.org/10.1016/j.optcom.2016.09.062.
[14] X. Wang, S. Lan, Optical properties of black phosphorus, Adv. Opt Photon 8 (2016) 618–655, https://doi.org/10.1364/AOP.8.000618.
[15] B. Li, C. Lai, G. Zeng, D. Huang, L. Qin, M. Zhang, M. Cheng, X. Liu, H. Yi, C. Zhou, F. Huang, S. Liu, Y. Fu, Black phosphorus, a rising star 2D nanomaterial in the post-graphene era: synthesis, properties, modifications, and photocatalysis applications, Small 15 (2019) 1804565, https://doi.org/10.1002/smll.201804565.
[16] F. Xia, H. Wang, J. Hwang, A.H. Castro Neto, L. Yang, Black phosphorus and its isoelectronic materials, Nat. Rev. Phys. 1 (2019) 306–317, https://doi.org/10.1038/s42254-019-0043-5.
[17] P. Luo, W. Wei, G. Lan, X. Wei, L. Meng, Y. Liu, J. Yi, G. Han, Dynamical manipulation of a dual-polarization plasmon-induced transparency employing an anisotropic graphene-black phosphorus heterostructure, Opt Express 29 (2021) 29690–29703, https://doi.org/10.1364/OE.435998.
[18] Y. Xu, H. Li, Y. Wu, L. Li, Z. Zhang, S. Qin, Broadband electromagnetically induced transparency-like manipulation of graphene–black phosphorus hybrid metasurface, J. Phys. D Appl. Phys. 54 (2021) 445104, https://doi.org/10.1088/1361-6463/ac1a9f.
[19] X.Q. Jiang, S.N. Chen, R.X. Sun, Z.B. Liu, Controllable graphene/black phosphorus van der Waals heterostructure tunneling device, Mater. Lett. 300 (2021) 130189, https://doi.org/10.1016/j.matlet.2021.130189.
[20] Y. Liu, M. Yang, J. Lu, Y. Liu, H. Liu, E. Zhang, W. Fu, J. Wang, Z. Hu, J. Yin, G. Eda, S. Wang, J. Yi, A. Vinu, K.P. Loh, Tuning photoresponse of graphene-black phosphorus heterostructure by electrostatic gating and photo-induced doping, Chin. Chem. Lett. 33 (2022) 368–373, https://doi.org/10.1016/j.cclet.2021.06.079.
[21] L. Cui, M. Sun, Graphene plasmon-enhanced polarization-dependent interfacial charge transfer excitons in 2D graphene-black phosphorus heterostructures in NIR and MIR regions, J. Phys. Chem. C 125 (2021) 22370–22378, https://doi.org/10.1021/acs.jpcc.1c07274.
[22] X. Zhang, C. Yan, X. Hu, Q. Dong, Z. Liu, W. Lv, C. Zeng, R. Su, Y. Wang, T. Sun, Z. Xing, C. Pang, B. Zhang, W. Shi, M. Long, High performance mid-wave infrared photodetector based on graphene/black phosphorus heterojunction, Mater. Res. Express 8 (2021) 035602, https://doi.org/10.1088/2053-1591/abed14.
[23] J. Xu, Y.J. Song, J.H. Park, S. Lee, Graphene/black phosphorus heterostructured photodetector, Solid State Electron. 144 (2018) 86–89, https://doi.org/10.1016/j.sse.2018.03.007.
[24] A. Gao, Z. Zhang, L. Li, B. Zheng, C. Wang, Y. Wang, T. Cao, Y. Wang, S. Liang, F. Miao, Y. Shi, X. Wang, Robust impact-ionization field-effect transistor based on nanoscale vertical graphene/black phosphorus/indium selenide heterostructures, ACS Nano 14 (2019) 434–441, https://doi.org/10.1021/acsnano.9b06140.
[25] G. Xiao, Z. Lin, H. Yang, Y. Xu, S. Zhou, H. Li, X. Liu, P. Wangyang, Tunable and anisotropic perfect absorber using graphene-black phosphorus nanoblock, Opt Express 30 (2022) 23198–23207, https://doi.org/10.1364/OE.461261.
[26] Y. Cai, K.D. Xu, N. Feng, R. Guo, H. Lin, J. Zhu, Anisotropic infrared plasmonic broadband absorber based on graphene-black phosphorus multilayers, Opt Express 27 (2019) 3101–3112, https://doi.org/10.1364/OE.27.003101.
[27] Q. Hong, F. Xiong, W. Xu, Z. Zhu, K. Liu, X. Yuan, J. Zhang, S. Qin, Towards high performance hybrid two-dimensional material plasmonic devices: strong and highly anisotropic plasmonic resonances in nanostructured graphene-black phosphorus bilayer, Opt Express 26 (2018) 22528–22535, https://doi.org/10.1364/OE.26.022528.
[28] C. Liu, H. Li, H. Xu, M. Zhao, C. Xiong, M. Li, B. Ruan, B. Zhang, K. Wu, Plasmonic biosensor based on excellently absorbable adjustable plasmon-induced transparency in black phosphorus and graphene metamaterials, New J. Phys. 22 (2020) 073049, https://doi.org/10.1088/1367-2630/ab9b58.
[29] X. Liu, C.R. Ryder, S.A. Wells, M.C. Hersam, Resolving the in-plane anisotropic properties of black phosphorus, Small Methods 1 (2017) 1700143, https://doi.org/10.1002/smtd.201700143.
[30] F. Zhou, C. Liang, Theoretical study of SPP properties based on black phosphorus–graphene van der Waals heterostructure, AIP Adv. 10 (2020) 115107, https://doi.org/10.1063/5.0025156.
[31] F. Zhou, All-optical plasmonic modulator based on graphene/black phosphorus heterostructure with angle-dependence in visible regime, Opt Commun. 530 (2023) 129122, https://doi.org/10.1016/j.optcom.2022.129122.
[32] L. Cui, J. Wang, M. Sun M, Graphene plasmon for optoelectronics, Rev. in Phys. 6 (2021) 100054, https://doi.org/10.1016/j.revip.2021.100054.
[33] X. Luo, T. Qiu, W. Lu, Z. Ni, Plasmons in graphene: recent progress and applications, Mater. Sci. Eng. R Rep. 74 (2013) 351–376, https://doi.org/10.1016/j.mser.2013.09.001.
[34] A. Islam, W. Du, V. Pashaei, H. Jia, Z. Wang, J. Lee, G.J. Y, X.H. Chen, P.X.L. Feng, Discerning black phosphorus crystal orientation and anisotropy by polarized reflectance measurement, ACS Appl. Mater. Interfaces 10 (2018) 25629–25637, https://doi.org/10.1021/acsami.8b05408.
[35] P. Luo, G. Lan, J. Nong, X. Zhang, T. Xu, W. Wei, Broadband coherent perfect absorption employing an inverse-designed metasurface via genetic algorithm, Opt Express 30 (2022) 34429–34440, https://doi.org/10.1364/OE.468842.
[36] Q. Bao, K.P. Loh, Graphene photonics, plasmonics, and broadband optoelectronic devices, ACS Nano 6 (2012) 3677–3694, https://doi.org/10.1021/nn300989g.
[37] L.A. Shiramin, D. Van Thourhout, Graphene modulators and switches integrated on silicon and silicon nitride waveguide, IEEE J. Sel. Top. Quant. 23 (2016) 94–100, https://doi.org/10.1109/JSTQE.2016.2586458.
[38] S.J. Koester, H. Li, M. Li, Switching energy limits of waveguide-coupled graphene-on-graphene optical modulators, Opt Express 20 (2012) 20330–20341, https://doi.org/10.1364/OE.20.020330.